Earthquakes and Structures, *Vol. 17, No. 1 (2019) 1-15*
DOI: https://doi.org/10.12989/eas.2019.17.1.001

Effects of pulse-like nature of forward directivity ground motions on the seismic behavior of steel moment frames

Iman Mansouri[1a], Shahrokh Shahbazi[2b], Jong Wan Hu[*3,4] and Salar Arian Moghaddam[5a]

[1]*Department of Civil Engineering, Birjand University of Technology, Birjand, Iran*
[2]*TAAT Investment Group, Tehran, Iran*
[3]*Department of Civil and Environmental Engineering, Incheon National University, Incheon 22012, South Korea*
[4]*Incheon Disaster Prevention Research Center, Incheon National University, Incheon 22012, South Korea*
[5]*International Institute of Earthquake Engineering and Seismology (IIEES), Tehran, Iran*

(Received December 26, 2018, Revised April 2, 2019, Accepted April 10, 2019)

Abstract. In the structures with high level of ductility, the earthquake energy dissipation in structural components is an important factor that describes their seismic behavior. Since the connection details play a major role in the ductile behavior of structure, in this paper, the seismic response of 3-, 5- and 8-story steel special moment frames (SMFs) is investigated by considering the effects of panel zone modeling and the influence of forward-directivity near-field ground motions. To provide a reasonable comparison, selected records of both near and far-field are used in the nonlinear time-history analysis of models. The results of the comparison of the median maximum inter-story drift under excitation by near-field (NF) records and the far-field (FF) ground motions show that the inter-story drift demands can be obtained 3.47, 4.86 and 5.92 times in 3-, 5- and 8-story structures, respectively, undergoing near-field earthquakes.

Keywords: special steel moment frame; forward directivity; inter-story drift; panel-zone, near-field

1. Introduction

Many researches have been conducted to explore the seismic behavior of structures (Farzampour 2019, Farzampour and Kamali-Asl 2015, Farzampour and Kamali Asl 2014, Khorami *et al.* 2017, Mansouri *et al.* 2016, Mirzai *et al.* 2018, Nastri *et al.* 2015, Nastri *et al.* 2017, Seo *et al.* 2012, Seo and Hu 2016, Seo *et al.* 2015a, Seo *et al.* 2015b, Seo and Shukla 2016, Zeynali *et al.* 2018). In the last two decades, the earthquake engineering research on the characterization of "distance to the site" has been limited. This scarcity has been due to the existence of some cases against conventional hypotheses of far-field (FF); another reason has been the limited documentary information including registered records in the near-field (NF) region (Shahbazi *et al.* 2018a, Shahbazi *et al.* 2018b, Shahbazi *et al.* 2019). Although historical registered records during the earthquakes of 1996 Park Field and 1971 San Fernando, California can be used as a starting point to study the destructive effects of near-field earthquakes (Veismoradi and Darvishan 2018), there was a considerable research interest in near-field earthquakes and their unique characteristics just after the occurrence of destructive earthquakes, including 1992 Lenders, 1994 Northridge, 1995 Kobe, and 1999 and Chi-Chi in Taiwan (Zhao *et al.* 2017). In the near-field area, ground motions are strongly affected by the faulting mechanism, slip direction to the site, and static displacement of the ground surface resulting from the fling step (Eskandari *et al.* 2017, Yazdani and Alembagheri 2017). The properties of near-field ground motions cause the released energy to appear at the beginning of time series resulting from faulting, like a continuous long-period pulse, and this strengthens the acceleration response spectrum in low frequencies (Ansari *et al.* 2018, Esfahanian and Aghakouchak 2015, Kalkan and Kunnath 2006). The effect of forward-directivity is created for strike-slip faults in the vertical direction on the slip, as in the case of the earthquake of Kobe Japan, or in vertical direction on the slip for dip-slip faults, such as during Chi-Chi Taiwan (Kalkan and Kunnath 2006). Due to the forward directivity and fling step, recorded motions near the active faults have different features relative to the ordinary recorded motions in the distance far from the fault (Nicknam *et al.* 2013). Each of these properties can cause different effects on structures. For example, the structures can be subjected to large deformation demands at the arrival of the velocity pulse, requiring the building to dissipate significant input energy in a single plastic cycle or relatively few plastic cycles. This demand will affect the buildings with restricted ductility capacity (Kalkan and Kunnath 2006). Furthermore, the evolution of residual ground displacement due to tectonic deformation is seen in the case of fling step (Kalkan and Kunnath 2006). Furthermore, energy accumulation in such ground motion excitations can cause a pulse-like motion in the short-term period and one pulse (Ashrafi *et al.* 2016, Beyen and Tanircan 2015). In other words, the maximum demands of deformation in near-field correspond to the minimum

∗Corresponding author, Ph.D.
E-mail: jongp24@inu.ac.kr
[a]Ph.D.
[b]Graduate Student Researcher

ISSN: 2092-7614 (Print), 2092-7622 (Online)

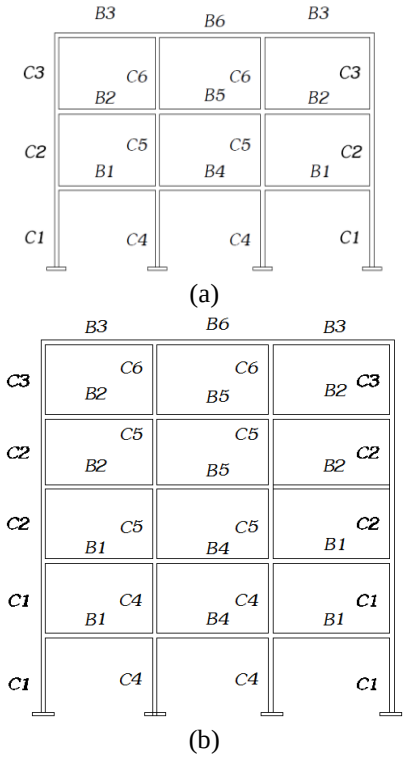

Fig. 1 (a) Model of a 3-story structure; (b) Model of a 5-story structure

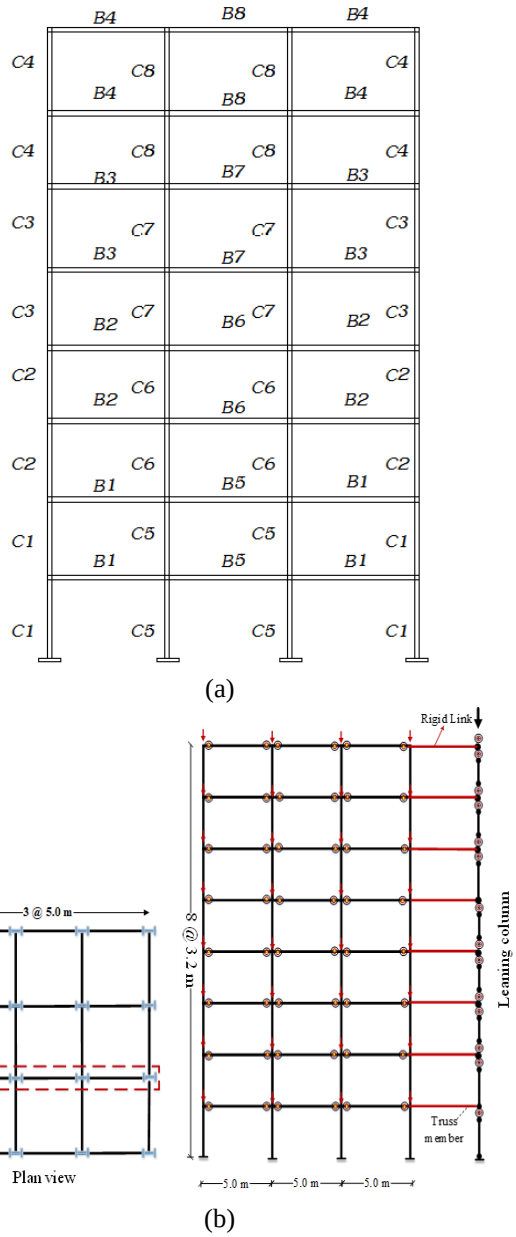

Fig. 2 (a) Model of a 8-story structures, (b) Typical details of nonlinear modeling

number of loading cycles (Khoshnoudian and Ahmadi 2013, Tajammolian *et al.* 2014). This effect has been observed in near-field records due to the existence of long-amplitude pulses with a long-term period, getting energy suddenly dissipate s in a short time period and in one or few cycles (Seo and Hu 2016). On the other hand, the energy of earthquake in a structural system gradually increases more undergoing motions far from the fault, which causes steady input and cumulative energy in a specific period. Several studies have evaluated the near-field effect on the response of structures: for instance, there has been research on the seismic performance of reinforced concrete (RC) structures under near-field records (Beiraghi *et al.* 2016, Eskandari *et al.* 2017, Moniri 2017, Mortezaei and Ronagh 2013). Seismic behavior of steel structures equipped with triple concave friction pendulum under near-field earthquakes was studied by Tajammolian *et al.* (2016) and Yin *et al.* (2017). Concerning the design concept based on performance, Gerami and Abdollahzadeh (2015) investigated the extent of vulnerability pertaining to steel moment frames that experienced near filed ground motions. Dimakopoulou *et al.* (2013) researched the impact of modeling hypothesis on the seismic reactions concerning structures subjected to near field records. The impact of forward directivity concerning the risk of collapse was investigated by Champion and Liel (2012). Rahgozar *et al.* (2017) investigated the actions of bracing frames of the self-centering type subjected to near field ground motions. The effects of near-field ground motions with pulse-like nature on the behavior of structure have not been clarified yet; the reason is that the number of near-field records is limited; in addition, the study of the structure's behavior undergoing these records cannot easily be performed using simplified models such as equivalent SDOF systems. Therefore, it is essential to study and compare the effects of these types of ground motions on different structural systems.

The aim of the present paper is to obtain explicit estimates of seismic demand for structures subjected to near-field earthquakes and to explore the effect of forward-directivity on the seismic performance of special moment frame. Although (Kalkan and Kunnath 2006) investigated the effect of near-field ground motions with forward-directivity on steel frames, that study focused on the intersory drift. By contrast, in the present study, maximum displacement, velocity and acceleration of each story, as well as inter-story drift and axial force of columns are obtained through an extensive numerical analysis and post-

Table 1 Sections of a 3-story structure

Column (length*width*thickness) mm	Beam	Section type
Tube 200×200×20	IPE* 300	C1 , B1
Tube 200×200×20	IPE 300	C2 , B2
Tube 200×200×20	IPE 270	C3 , B3
Tube 280×280×20	IPE 400	C4 , B4
Tube 280×280×20	IPE 300	C5 , B5
Tube 280×280×20	IPE 270	C6 , B6

Table 2 The sections of 5-story structure

Column	Beam	Section type
Tube 240×240×20	IPE 360	C1 , B1
Tube 240×240×20	IPE 360	C2 , B2
Tube 180×180×20	IPE 240	C3 , B3
Tube 340×340×20	IPE 400	C4 , B4
Tube 300×300×20	IPE 400	C5 , B5
Tube 240×240×20	IPE 240	C6 , B6

processing. Moreover, in order to obtain more realistic results, the panel zone element is considered for all models.

2. Characteristics of models

In the present study, three models (of 3-, 5- and 8-story buildings) were designed assuming type 3 soil (175 m/s≤V_s (shear-wave velocity)≤375 m/s) for their site location in order to evaluate seismic behavior of special steel moment frames. Seismic design of these structures was carried out according to Iranian Standard 2800 (BHRC 2014) using the ETABS software. The constructed 3D models had three longitudinal spans and three spans in the transverse direction with the equal length of 5 m and the identical height of 3.2 m for each story extracted from (Etemadi Mashhadi 2015). Staggered beaming was considered for the roof. The same type of columns and beams was considered on both sides in order to identify performance. All employed profiles were IPE- and box-shaped tubes for beams and columns, respectively (based on European standard profiles). Fig. 1 and Fig. 2 illustrate the 2D view of the 3, 5, 8-story model, while the used sections are listed in Tables 1-3.

As can be seen in Fig. 2(b), the leaning columns with gravity loads were linked to the frame by rigid elements to simulate *P*-Δ effects. The 2D models did not reflect the actual amount of vertical forces producing the overall overturning effects, because the gravity loads were directly applied by the tributary area of the loads acting on the 2D frame (Landolfo *et al.* 2017). Therefore, in order to consider the effect given by the complement of vertical loads, a leaning column was modeled (see Fig. 2(b)). This type of column was made of truss elements with flexural releases at both ends and did not contribute to lateral stiffness (PEER/ATC-72-1 2010). The following assumptions were considered in the design process. First, for all models, dead and live loads were considered as 65 and 20 kN/m^2, respectively. Second, dead and live loads for roof were considered 54 and 15 kN/m^2, respectively, in all cases.

Table 3 Sections of a 8-story structure

Column	Beam	Section type
Tube 340×340×20	IPE 450	C1 , B1
Tube 340×340×20	IPE 450	C2 , B2
Tube 280×280×20	IPE 450	C3 , B3
Tube 200×200×20	IPE 360	C4 , B4
Tube 400×400×20	IPE 450	C5 , B5
Tube 400×400×20	IPE 450	C6 , B6
Tube 340×340×20	IPE 450	C7 , B7
Tube 280×280×20	IPE 360	C8 , B8

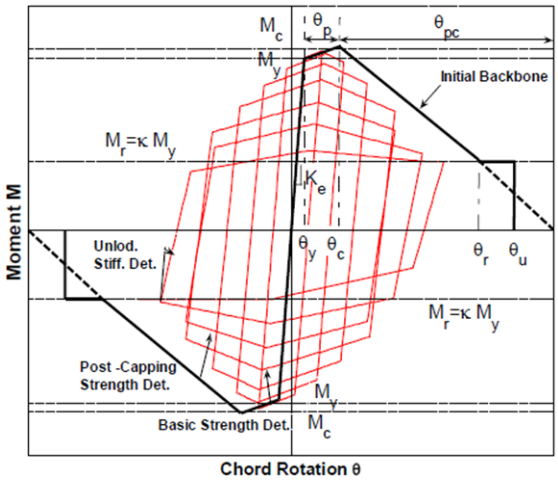

Fig. 3 Modified Ibarra-Medina-Krawinkler deterioration model (Lignos and Krawinkler 2009)

Third, the rigid diaphragm was considered for all stories. In the present study, the OpenSees software was used in order for structural modeling. The nonlinear behavior was considered using the concentrated plasticity concept with rotational springs (beams and columns were simulated using elastic elements). The behavior of rotational springs was introduced based on a bilinear hysteretic material. In OpenSees, the Bilin Material imitates the modified Ibarra-Medina-Krawinkler deterioration model with bilinear hysteretic response. Fig. 3 shows the parameters of Bilin Material in OpenSees. The relationships between variables were developed by (Lignos and Krawinkler 2009). In the literature, several analytical models for panel zone in terms of shear force-shear distortion relations have been proposed. In the present study, the Krawinkler panel zone model was adopted (see Fig. 4) which was also used in the AISC code.

Due to opposing moments within beams and columns, the panel zone is initially deformed in shear. The method presented by Gupta and Krawinkler (1999) was used to explicitly model the panel zone as a rectangle consisting of eight rigid elastic column-beam components and a rotational spring to denote shear disfigurements within the panel zone.

The fundamental periods of 3-, 5- and 8-story buildings were 0.48, 0.91, and 0.78 seconds, respectively.

The structures under research were modelling using elastic column-beam components which were linked through rotational springs to denote the nonlinear actions of the structures. The springs adhered to a bilinear hysteretic

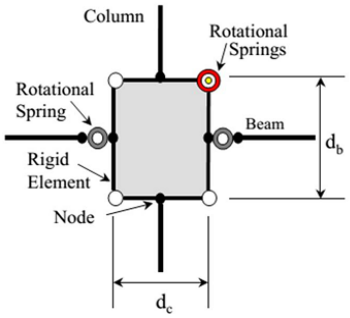

Fig. 4 Mathematical model of the panel zone (Gupta and Krawinkler 1999)

Table 4 The first three modes of vibration for benchmark buildings (Ohtori *et al.* 2004) (numbers in parentheses show the values of OpenSees results)

Benchmark structures	T_1	T_2	T_3
3-story	1.01 (1.01)	0.33 (0.34)	0.17 (0.19)
9-story	2.27 (2.28)	0.85 (0.87)	0.49 (0.52)

reaction on the basis of the adjusted Ibarra Krawinkler Deterioration Model. A rotational spring which was placed at the center of the reduced beam sections i.e., RBS was used to model the plastic hinge. The spring and panel zone were connected using an elastic column-beam component. The rigidity of such components had to be adjusted since a frame member was modeled as an elastic element which was linked in series with rotational springs at all ends in order for the equivalent rigidity of the framework to be equivalent to the rigidity of the actual frame member.

Since the verification study is essential for any numerical study, we followed the modeling methodology for benchmark structures previously proposed by (Ohtori *et al.* 2004). The first three modes of vibration for 3- and 9-story benchmark buildings are shown in Table 4. The results demonstrate that the modeling technique was correct.

3. Near-field ground motions including forward-directivity effect

The fault geometry position related to the considered place is vital in near field seismic occurrences in addition to the failure process and faulting type. The acquired reaction stemming from ground velocity amidst earthquakes exhibits a pulse-type shape of long periods denoting an action similar to a strike (Decanini *et al.* 2000). The pulse amplitude is dependent on failure propagation directivity towards the site. In the case that the fault failure is spread to the place in question, due to the failure propagation velocity is almost equal to the shear wave propagation velocity, the waves will reach this place within a short period of time leading to a pulse with great amplitude and longer period. Such phenomenon is referred to as forward-effect directivity. Then, in the case that the failure is getting further away from the site, the waves will end up in a scattered pattern, referred to as backward directivity, whilst

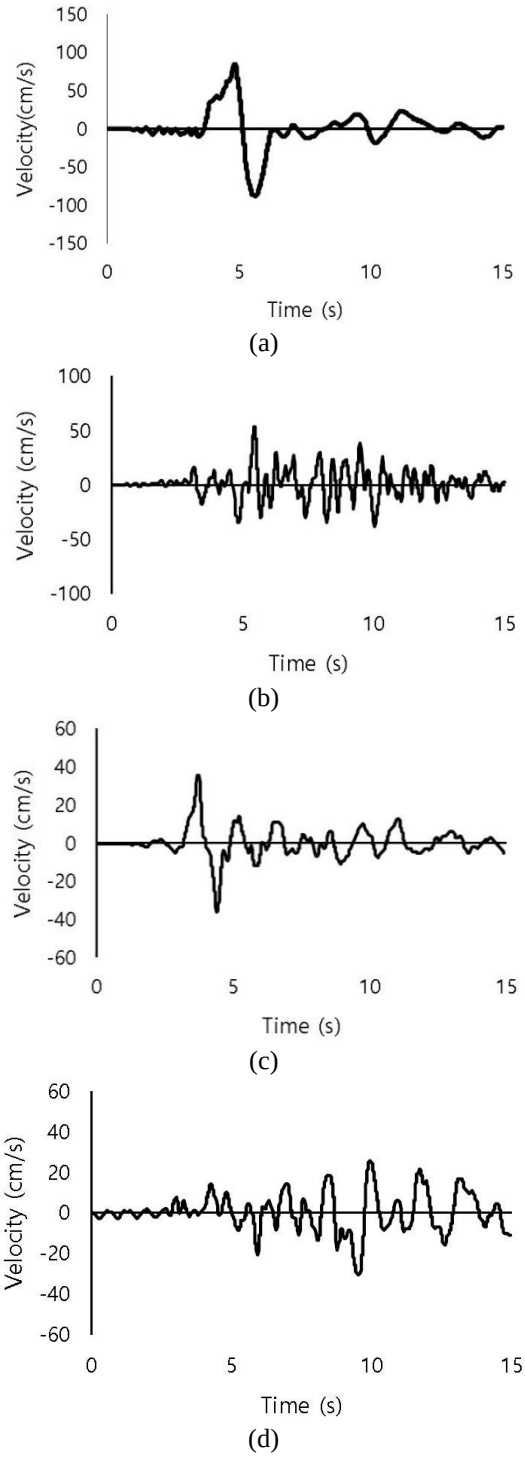

Fig. 5 Time histories of velocity in (a) forward directivity type: Northridge record: West Pico Canyon RD station (R=7.1 km) (b) non-forward directivity type: Loma Preita: Bran station (R=10.7 km) (c) forward directivity type: Loma Preita: Gilroy History Building station (R=12.7 km) and (d) non-forward directivity type: Loma Preita: Joshua Tree station (R=11.03 km) databases (Gillie *et al.* 2010)

the failure directivity will not be close nor away from the desired location. Such occurrence is referred to as neutral directivity (Singh 1985). Permanent ground displacement caused by surface failure may also result in pulse motion.

Table 5 Near field (NF) records

No	Year	Event	Station	*Vs*30 (m/sec)	mechanism	*Mw*	PGA(g)
1	1992	Erzican	Erzican	352.05	strike slip	6.69	0.49
2	1979	Imperial Valley	EC County Center FF	192.05	strike slip	6.53	0.22
3	1979	Imperial Valley	Meloland Geot. Array	264.57	strike slip	6.53	0.32
4	1995	Kobe	KJMA	312	strike slip	6.9	0.85
5	1995	Kobe	Port Island (0 m)	198	strike slip	6.9	0.38
6	1989	Loma Prieta	Saratoga - W Valley Coll	347.9	Reverse Oblique	6.93	0.4
7	1994	Northridge-01	Newhall - W Pico Canyon Rd	285.93	Reverse	6.69	0.43

Table 6 Far field (FF) records

No.	Event	Year	Record length (s)	Station	PGA (g)	*Mw*
1	Imperial Valley-06	1979	37.845	Calexico, Fire Station	0.27	6.5
2	Imperial valley	1979	100	Delta	0.35	6.5
3	Kocaeli_ Turkey	1999	27.2	Kocaeli- Duzce	0.36	7.5
4	Landers	1992	60	Palm Springs, Airport	0.075	7.2
5	Landers	1992	44	Yermo Fire station	0.24	7.3
6	Loma Prieta	1989	40	Loma Prieta Gilroy Array #3	0.56	6.9
7	Loma Prieta	1989	39.995	Coyote Lake Dam, downstream	0.18	7.1

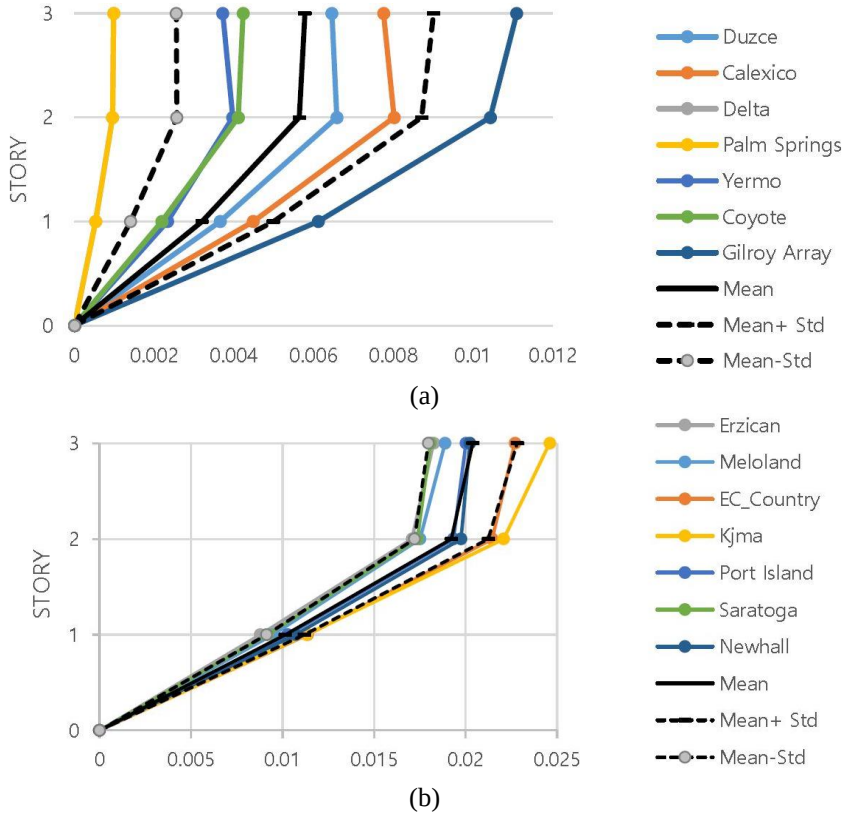

Fig. 6 Maximum story drifts of a 3-story building undergoing (a) far-field earthquakes; (b) near-field earthquakes

Such pulses differ from the ones created by forward directivity (Decanini *et al*. 2000).

This paper examines the pulse impact created through forward directivity which exerts the greatest extensive damage to the structure, according to prior studies (Alavi and Krawinkler 2004, Kalkan and Kunnath 2006).

High-intensity velocity pulses is one of the important features of near-field motions having forward directivity (see Fig. 5; see also Gillie *et al*. 2010).

4. Selection of ground motions

In time history analyses, choosing a suitable record is essential to evaluate structures. In the present study, seven ground motions were recorded in near-field with distinct forward directivity pulses. The ground motions including the forward directivity feature were taken from (Alavi and Krawinkler 2004, Bray and Rodriguez-Marek 2004). Seven records of far-field earthquakes were selected in order to perform the nonlinear time-history analysis. Far-field

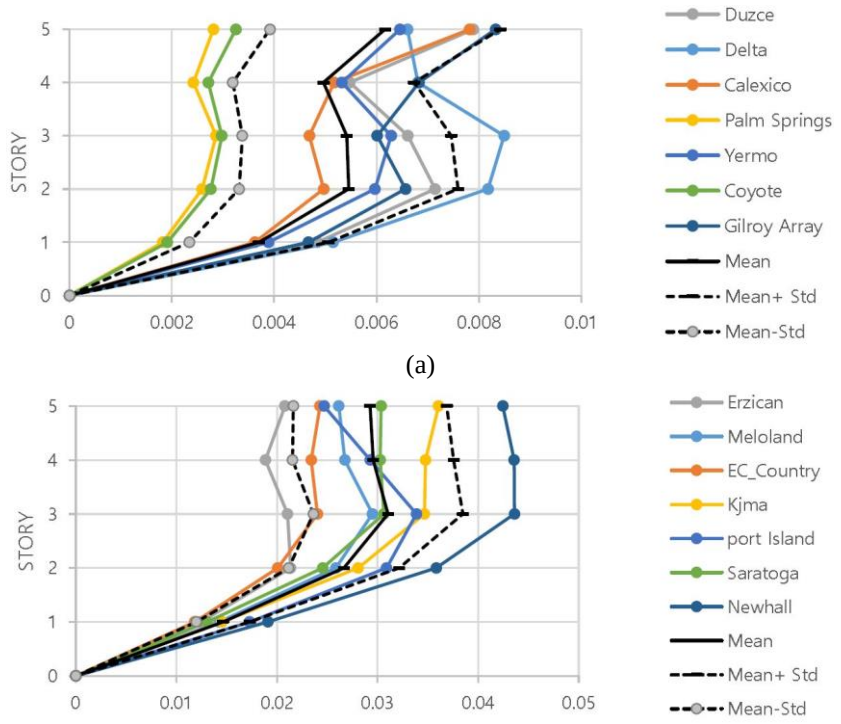

(a)

(b)

Fig. 7 Maximum story drifts of a 5-story building undergoing (a) far-field earthquakes; (b) near-field earthquakes

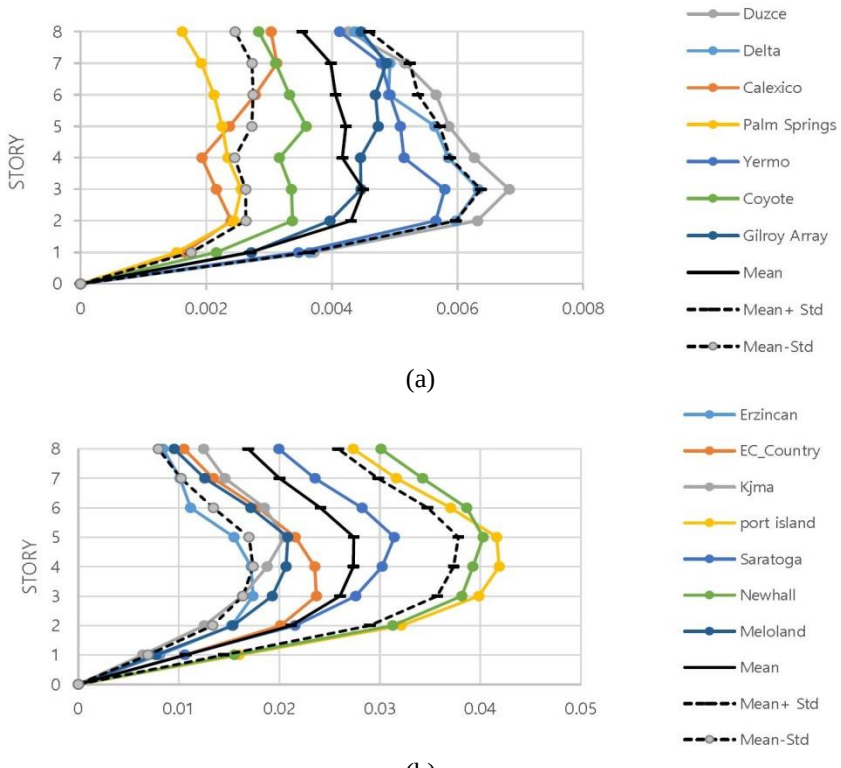

(a)

(b)

Fig. 8 Maximum story drifts of a 8-story building undergoing (a) far-field earthquakes; (b) near-field earthquakes

earthquakes were recorded from the distance of longer than 100 kilometers from the fault. The moment magnitude of these records was 6.5 to 7.5. The magnitude of near-field earthquakes was 6.53 to 6.93 and was recorded from the distance of lower than 10 km from the fault. Investigated records were recorded in type 3 soil (175 m/s$\leq V_s$ (shear-wave velocity) $\leq$375 m/s) in accordance with Iranian Standard 2800 (BHRC 2014) definition. Tables 5-6 summarize the general features of the selected ground motions.

Table 7 Comparison of the IDRM under far and near-field earthquakes

No. of story	Far fault (FF)			Near-field (NF)			NF/FF
	value	record	location	value	record	location	
3	0.011	Loma Prieta- Gilroy Array #3	Story 3	0.045	Kobe- Kjma	Story 3	4
5	0.008	Imperial Valley– Delta	Story 3	0.044	Northridge -Newhall pico Canyon	Story 3	5
8	0.007	Kocaeli- Duzce	Story 3	0.042	Kobe -Portisland	Story 4	6

Table 8 Comparison of average values of maximum drift undergoing far and near-field earthquakes

No. of story	Far-field (FF)	Near-field (NF)	NF/FF
3	0.005	0.02	3.47
5	0.006	0.03	4.86
8	0.004	0.02	5.92

Table 9 Comparison of the average maximum displacement of roof undergoing far and near-field earthquakes (m)

No. of story	FF	NF	NF/FF
3	0.045	0.158	3.45
5	0.071	0.405	5.71
8	0.089	0.538	6.02

Table 10 Comparison of the average axial value of the first story columns undergoing far and near-field earthquakes

No. of story	FF (ton)	NF (ton)	NF/FF
3	14.20	33.66	2.37
5	16.08	42.48	2.64
8	19.85	44.49	2.24

5. Evaluation of seismic response

Generally, 42 non-linear time history analyses were performed concerning 14 mentioned records, and the total models were considered. Maximum inter-story (IDRM) drift was used as the first engineering demand parameter to assess the overall level of system requirements. The value of IDRM is shown in Figs. 6-8 resulting from nonlinear time history analyses under two sets of records for special moment frames (3, 5, and 8-story).

By comparing the IDRM values in a 3-story structure (see Table 7), it can be observed that the maximum value of drift is yielded by the earthquake record of Loma Prieta-Gilroy Array #3 in the third story, under far-field ground motions, where the value is 0.011. On the other hand, in near-field events, the maximum value of IDRM is in the third story under the Kobe-Kjma earthquake by the amount of 0.045, i.e., 4 times more than the corresponding earthquake in far-field (NF) earthquake.

By comparing the IDRM values in a 3-story structure (see Table 7), it can be observed that the maximum value of drift is yielded by the earthquake record of Loma Prieta-Gilroy Array #3 in the third story, under far-field ground motions, where the value is 0.011. On the other hand, in near-field events, the maximum value of IDRM is in the third story under the Kobe-Kjma earthquake by the amount of 0.045, i.e., 4 times more than the corresponding earthquake in far-field (NF) earthquake.

In a 5-story building, the maximum of drift is 0.0436 and, under the earthquake record of Northridge-Newhall Pico canyon, which has forward directivity, happening at third story of structure, while, in this structure, the maximum amount of drift undergoing far-field earthquakes is 0.008492 under the Imperial Valley–Delta ground motion. In a 5-story structure, the maximum drift under the near-field earthquakes is more than 5 times of the corresponding amount of that under the far-field earthquakes (see Table 7). In a 8-story building, the maximum value of drift under the earthquake record of Kobe-Portisland, has forward directivity and occurs at the fourth story, is 0.0418, while this structure tolerates the maximum value of drift of 0.0068 undergoing far-field earthquakes and under the Kocaeli- Duzce record. In an 8-story structure, the maximum drift undergoing far-field earthquakes is more than six times of the corresponding amount of that under the far-field earthquakes (see Table 7). Furthermore, the comparison of average values of maximum drift for far and near-field earthquakes is shown in Table 8. From Figs. 6 to 8, it can be concluded that the middle stories are more likely to be subjected to damage, and the accumulation of vulnerability is seen in these stories. Tables 7 and 8 show that, for all studied frames, the inter-story demand is much higher in the case of NF records. The ratio of the inter-story drift NF to FF is increases with an increase of the height of the structure. Said differently, this ratio is proportional to the height of the structure. Moreover, based on Iranian Standard 2800 (BHRC 2014), the allowable inter-story drift for 3- and 5-story buildings is 0.025; for 8-story buildings, this value is 0.02. The results shown in Tables 7-8 demonstrate that inter-story drift exceeds the allowable value in the case of NF records.

Table 9 shows the comparison of the maximum value of roof displacement maximum displacement of roof undergoing far and near-field earthquakes undergoing far and near-field earthquakes specified that near-field ones accompanied with directivity in 3-story building produce the maximum displacement of 0.1834 m in the story of the roof that in comparison with the values of 0.084 of far-field earthquakes is more than 2.18 times. In a 5-story building, it produces the maximum displacement value of 0.5851 m, which is 5.3 times more than that the value of 0.11 in far-field earthquakes. In an 8-story building, these values are 0.8396 and 0.1290 m for near and far-field earthquakes, respectively, so the difference is about 6.5 times.

Comparing the values of axial force of columns undergoing far and near-field earthquakes (Table 10) suggests that, in near-field earthquakes accompanied with directivity, the maximum axial force in first story column is 39.84, 49.87 and 59.34 tons in 3, 5 and 8-story buildings,

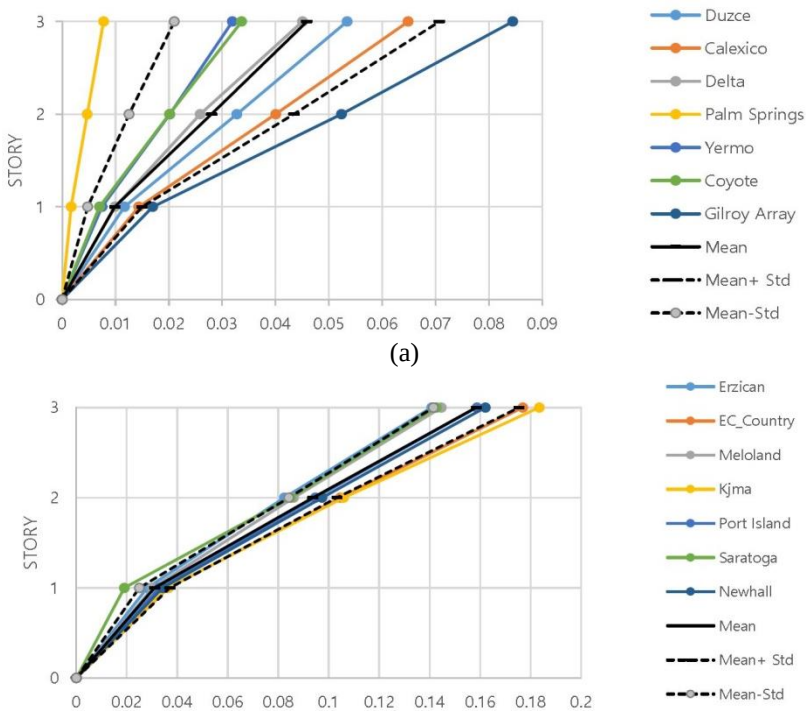

Fig. 9 Maximum displacements of a 3-story building undergoing (a) far-field earthquakes; (b) near-field earthquakes

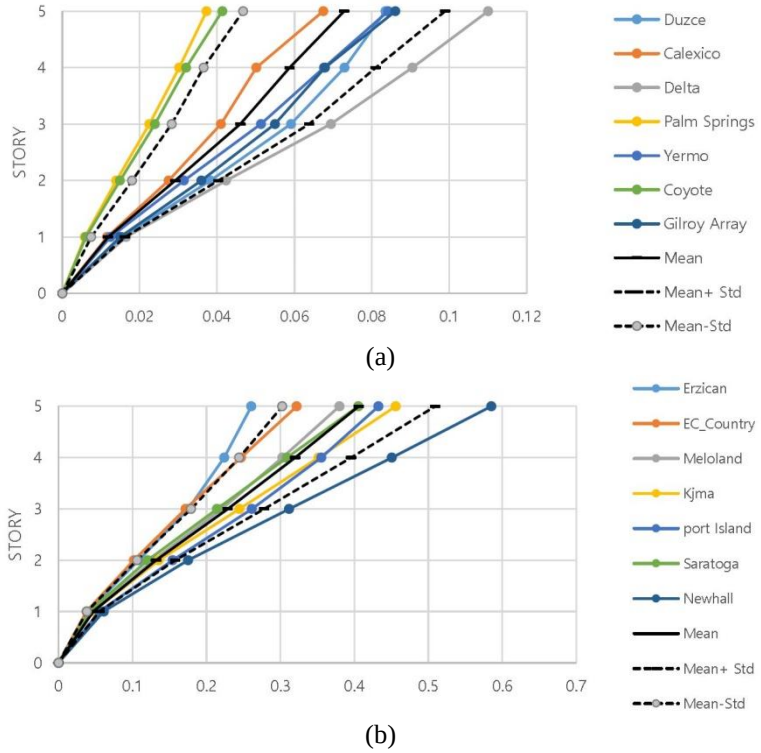

Fig. 10 Maximum displacements of a 5-story building undergoing (a) far-field earthquakes; (b) near-field earthquakes

Table 11 Comparison of the average value of base shear force undergoing far and near-field earthquakes (ton)

No. of story	FF (ton)	NF (ton)	NF/FF
3	116.40	147.75	1.27
5	182.80	286.01	1.56
8	334.47	566..97	1.69

respectively. In addition, the values undergoing the far-field records are 27.603, 22.618, and 26.23 tons, respectively. Therefore, the axial force of the first story is 1.44, 2.2 and 2.26 times higher in 3, 5 and 8-story buildings.

Table 11 shows the base shear values undergoing far and near-field earthquakes. In near-field earthquakes

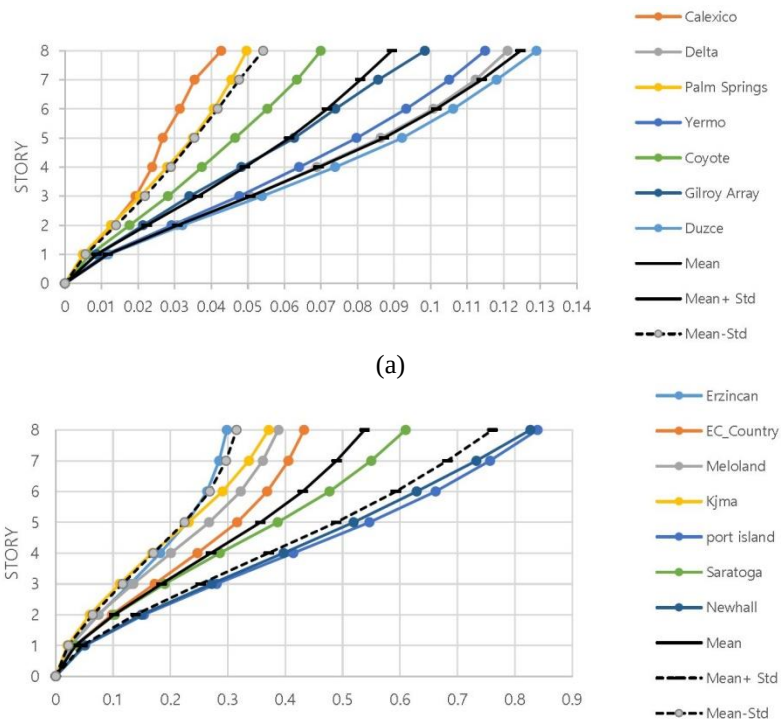

(a)

(b)

Fig. 11 Maximum displacements of a 8-story building undergoing (a) far-field earthquakes; (b) near-field earthquakes

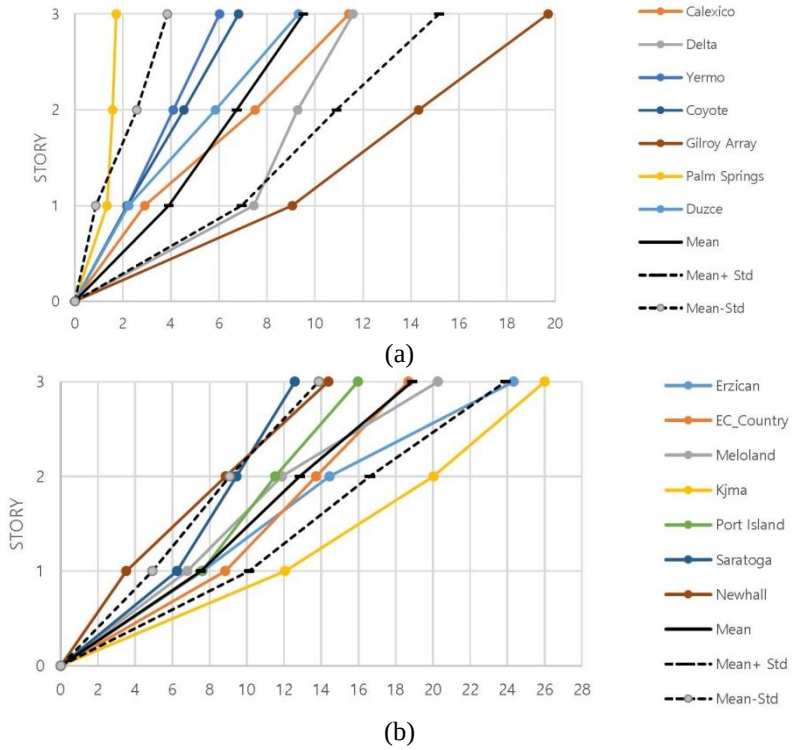

(a)

(b)

Fig. 12 Maximum accelerations of a 3-story building undergoing (a) far-field earthquakes; (b) near-field earthquakes

accompanied with directivity, the maximum value of base shear of the first story is 158.75, 296.12, and 616.67 tons for 3-, 5- and 8-story buildings, respectively. Furthermore, these values are 134.36, 227.13, and 389.41 tons undergoing far-field records, respectively. Therefore the base shear force is 1.18, 1.3 and 1.58 times higher in 3-, 5- and 8-story structures.

The value of maximum acceleration is illustrated in Fig. 12-resulting from nonlinear dynamic analyses under two groups of earthquake records for buildings with a special moment frame system (3, 5 and 8-story) undergoing both groups of earthquake records.

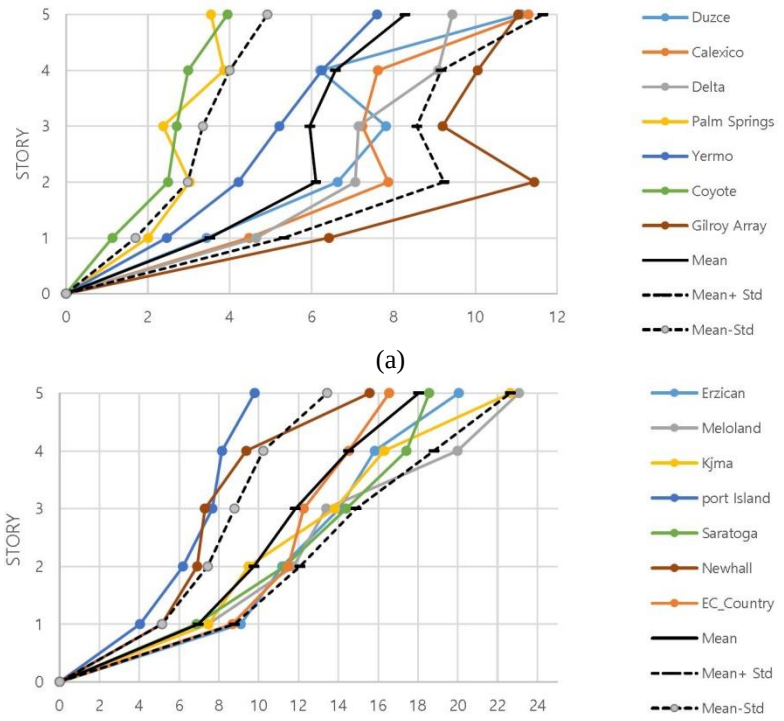

Fig. 13 Maximum accelerations of a 5-story building undergoing (a) far-field earthquakes; (b) near-field earthquakes

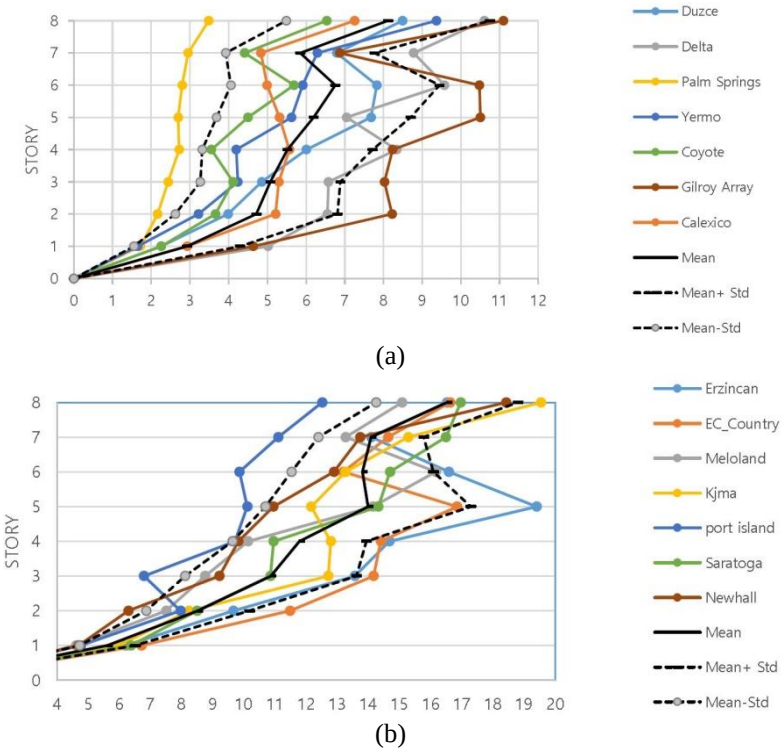

Fig. 14 Maximum accelerations of a 8-story building undergoing (a) far-field; (b) near-field earthquakes

A comparison of the maximum acceleration values of stories undergoing near and far-field earthquakes suggests that the maximum acceleration of story, in the near-field earthquakes accompanied with directivity, is 26 m/s^2 (its location in story 3 undergoing Kobe-Kjma record), 23 m/s^2 (its location in story 5 undergoing Imperial valley-Meloland record), and 19.54 m/s^2 (its location in story 8 undergoing Kobe-Kjma record) in 3, 5 and 8-story buildings, respectively; at he same time, these values in structures undergoing far-field records are 19.71, 11.43, and 11.09 m/s^2, respectively, undergoing Loma Prieta-Gilroy Array #3.

Table 12 Building weight (kg)

Building/Story No.	1	2	3	4	5	6	7	8
3-story	3537.40	3365.81	3172.94	-	-	-	-	-
5-story	4262.73	4482.26	4130.67	3440.70	2836.09	-	-	-
8-story	5405.28	5483.74	5483.74	5061.15	4884.30	4262.73	3766.99	2849.33

Table 13 Comparison of observed floor demands in models with the corresponding design level values for a 3-story building

3-story					$acc._{demand}/acc._{design}$	
Story	F_p (kg)	Designed floor acc. (g)	max demand acc. (NF) (g)	max demand acc. (FF) (g)	NF	FF
STORY3	23086.77	0.74	2.65	2.01	3.57	2.71
STORY2	22638.87	0.69	2.04	1.46	2.98	2.13
STORY1	19119.80	0.55	1.23	0.92	2.23	1.68

Table 14 Comparison of observed floor demands in models with the corresponding design level values for a 5-story building

5-story					$acc._{demand}/acc._{design}$	
Story	F_p (kg)	Designed floor acc. (g)	max demand acc. (NF) (g)	max demand acc. (FF) (g)	NF	FF
STORY5	25292.17	0.91	2.35	1.15	2.59	1.27
STORY4	29037.00	0.86	2.04	1.02	2.37	1.19
STORY3	29335.06	0.72	1.47	0.94	2.03	1.29
STORY2	26496.43	0.60	1.20	1.17	1.99	1.93
STORY1	21154.88	0.51	0.93	0.65	1.83	1.29

Table 15 Comparison of observed floor demands in models with the corresponding design level values for a 8-story building

8-story					$acc._{demand}/acc._{design}$	
Story	F_p (kg)	Designed floor acc. (g)	max demand acc. (NF) (g)	max demand acc. (FF) (g)	NF	FF
STORY 8	22483.34	0.80	1.99	1.13	2.48	1.41
STORY 7	28184.80	0.76	1.68	0.90	2.20	1.17
STORY 6	28544.40	0.68	1.69	1.07	2.48	1.57
STORY 5	28678.97	0.60	1.98	1.07	3.31	1.79
STORY 4	26343.90	0.53	1.50	0.85	2.82	1.60
STORY 3	25083.71	0.47	1.44	0.82	3.10	1.76
STORY 2	22135.29	0.41	1.17	0.84	2.85	2.04
STORY 1	19227.72	0.36	1.72	0.51	4.74	1.41

Diaphragms shall be designed to resist the lateral seismic forces determined by the following formula (see Eq. (1))

$$F_{pui} = \frac{\sum_{j=i}^{n} F_{uj}}{\sum_{j=i}^{n} W_j} W_i \quad (1)$$

where F_{pui}=the lateral load in the diaphragm, at level i, and W_i is the weight of the diaphragm and its attachments, F_{uj} and W_j are the story farce and story weight and n is number of stories.

Newton's second law of motion is employed to calculate the designed floor acceleration. Tables 12-15 show the assumptions and details of calculation to obtain the designed floor acceleration. The results reveal that, in both types of records (NF and FF), the maximum demanded acceleration obtained from time history analysis is higher than floor acceleration designed by the Iranian Standard 2800 (BHRC 2014).

Figs. 15-17 show the value of maximum velocity resulting from nonlinear time history analyses under two groups of earthquake records for buildings with a special moment frame system (3, 5 and 8-story) undergoing both groups of earthquake records.

Comparing the maximum velocity values of stories undergoing near and far-field earthquakes suggests that the maximum velocity of story, in the near-field earthquakes accompanied with directivity, is 1.95 m/s^2 (its location in story 3 undergoing Kobe-Kjma record), 2.35 m/s^2 (its location in story 5 undergoing Kobe-Kjma record), and 2.44 m/s^2 (its location in story 8 undergoing Northridge-Newhall Pico Canyon record) in 3-, 5- and 8-story buildings, respectively; furthermore, these values in the structures undergoing far-field records are 1.14 m/s (its location in story 3 undergoing Loma Prieta- Gilroy #3 record), 1.06 m/s (its location undergoing Imperial Valley-Delta record), and 1.029 m/s (undergoing Kocaeli- Duzce record), respectively.

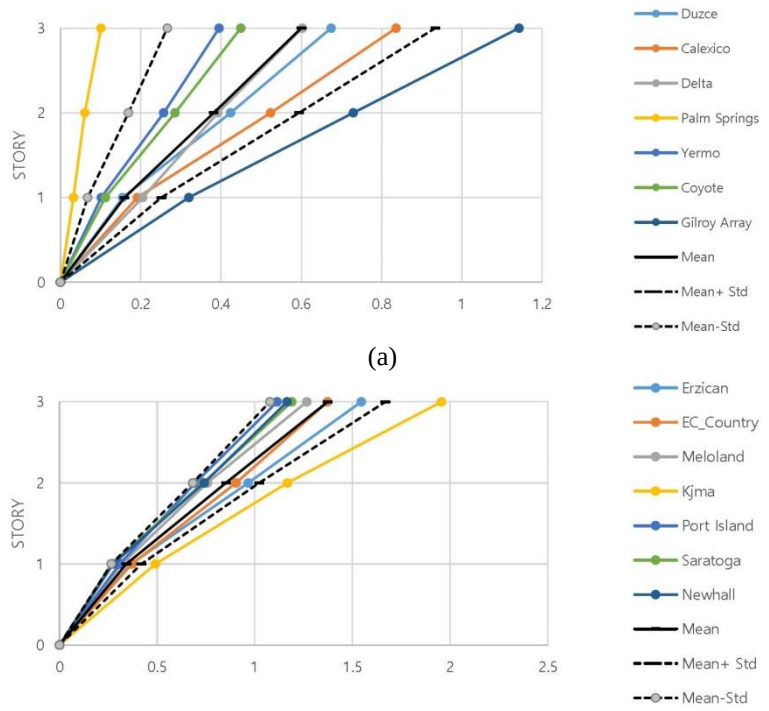

(a)

(b)

Fig. 15 Maximum velocities of a 3-story building undergoing (a) far-field earthquakes; (b) near-field earthquakes

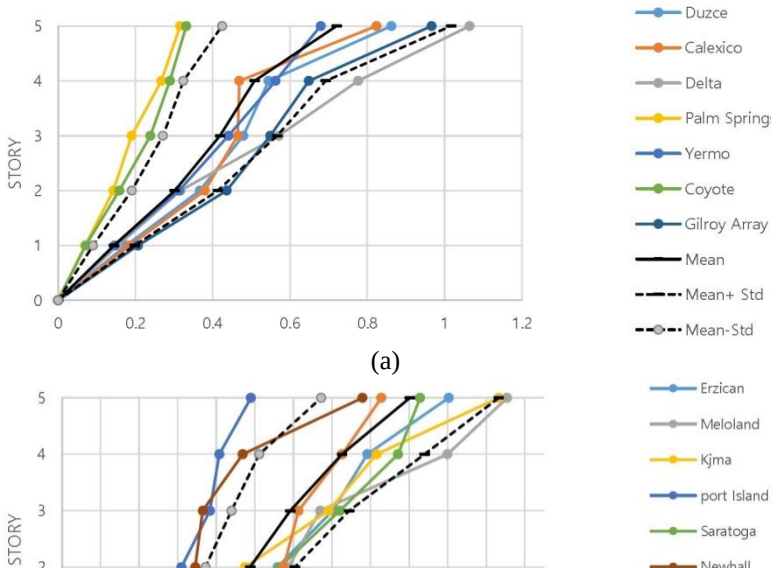

(a)

(b)

Fig. 16 Maximum velocities of a 5-story building undergoing (a) far-field earthquakes and (b) near-field earthquakes

6. Conclusions

Although the observed damage and rupture of engineering structures demonstrated the vulnerability of current buildings to near-field earthquakes during last earthquakes, there are still unknown parameters describing the consequences of near-field ground motions on the response of the structures which are anticipated to have a high level of ductility. Present codes do not appropriately consider the influences of these long-period pulses in the design procedure. Simple methods of determination of non-elastic requirements through magnifying design spectrum

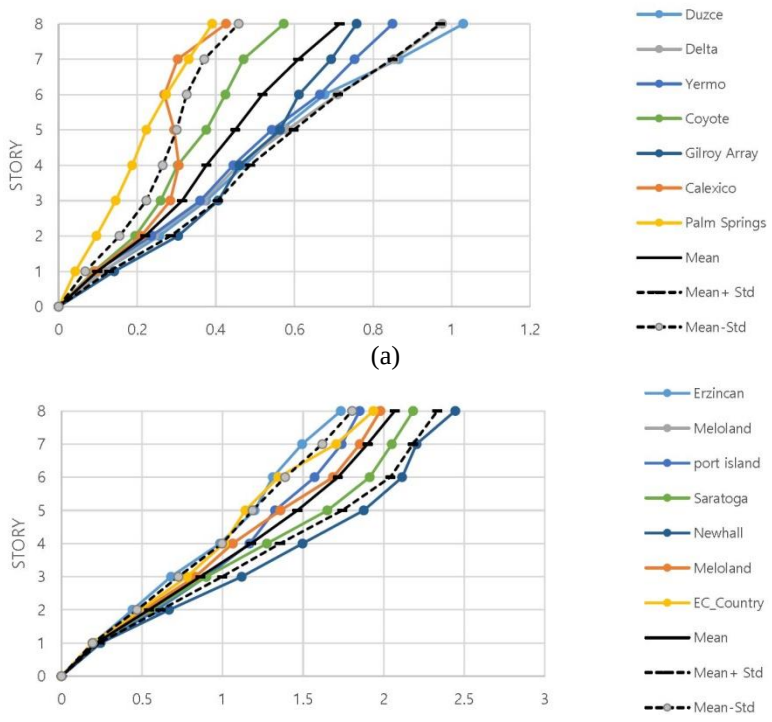

Fig. 17 Maximum velocities of a 8-story building undergoing (a) far-field earthquakes; (b) near-field earthquakes

cannot properly estimate acceptable responses for near-field earthquakes. Therefore, in the present paper, our aims was to investigate the response of specific moment frames considering the effects of modeling panel zone on near-field motions and the amount of variation among these responses with far-fault earthquakes.

The evaluation process conducted in this study showed that steel moment frame buildings required to show special ductility were influenced by large displacement demands in the presence of velocity pulse of forward directivity effects. This issue requires that the structure dissipates a great amount of seismic energy in one or more limited plastic cycles.

This requirement requires a structure with restricted ductility capacity, which is against their design philosophy (high ductility and naturally more energy dissipation). In contrast, the far-fault motions gradually entered the input energy and, through the displacement demands, are on average less than the ones in near-field record; as a result, the structural system is influenced more by plastic cycles.

• The results of the comparison between the median maximum drift undergoing near-field records with influence forward-directivity and far-fault earthquake demonstrate that the amount of drift was 3.47, 4.86 and 5.92 times higher in 3-, 5- and 8-story structures, respectively. In general, the inter-story drift under the influence of near-field earthquakes was larger in comparison with far-field records. The ratio of the inter-story drift NF to FF increased with an increase of the height of the structure. Said differently, this ratio was proportional to the height of the structure. On the other hand, under the influence of near-field earthquakes, in all three structures, the values of inter-story drifts exceeded the allowable values of the Iranian Standard 2800, which necessitates an overview of the allowable values of the drifts in this code.

• The comparison between the maximum mean of roof displacement undergoing near-field records with the influence of forward-directivity and far-fault earthquakes showed that the roof displacement was 3.45, 5.7 and 6 times higher in 3-,5-, and 8-story buildings, respectively undergoing near-field earthquakes. It can be clearly seen that, in NF records, the roof displacement was higher than in FF earthquakes. On the other hand, the story displacement increased along with the height of building.

• The comparison between the mean values of axial force of first story columns undergoing near-area records with the influence of forward-directivity and far-fault earthquakes showed that the axial force of first story columns was 2.37, 2.64, and 2.40 times higher in 3-, 5- and 8-story structures undergoing near-field earthquakes, respectively.

• The comparison between the average of maximum acceleration of stories undergoing near-field records with the influence of forward-directivity and far-fault earthquakes showed that the stories acceleration was 1.98, 2.15, and 2.10 times higher in 3-, 5- and 8-story structures undergoing near-field earthquakes, respectively. Since the story acceleration is an important factor for the non-structural components the story acceleration demands was compared with the values of the designed floor acceleration. The results show the assumptions and details of calculation used to obtain the designed floor acceleration. The results reveal that, in both types of records (NF and FF), the maximum

demanded acceleration obtained from time history analysis was higher than floor acceleration designed by the Iranian Standard 2800.

• The comparison between the mean of the maximum velocity of stories undergoing near-field records with the influence of forward-directivity and far-fault earthquakes showed that the stories velocity was 2.28, 2.78, and 2.83 times higher in 3-, 5-, and 8-story structures undergoing near-field earthquakes, respectively.

• The comparison between the mean of base shear undergoing near-field records with the influence of forward-directivity and far-fault earthquakes showed that the base shear was 1.26, 1.56 and 1.69 times higher in 3-, 5- and 8-story structures undergoing near-field earthquakes, respectively. One of the important parameters for structural engineers is the base shear. The results of nonlinear analysis showed that the story shear was higher in the effect of NF records in comparison with FF records. The story shear ratio (NF/FF) increased with an increase of the height of the structure.

The results of the numerical modeling performed in this paper showed that steel specific moment-frame buildings are influenced by large displacement demands in the presence of velocity pulse in time-history velocity. This issue requires that the structure dissipates a great deal of energy in one or more plastic cycle.

Acknowledgments

This research was supported by Basic Science Research Program through the National Research Foundation of Korea (NRF) funded by the Ministry of Science, ICT & Future Planning (2017R1A2B2010120).

References

Alavi, B. and Krawinkler, H. (2004), "Behavior of moment-resisting frame structures subjected to near-fault ground motions", *Soil Dyn. Earthq. Eng.*, **33**(6), 687-706. https://doi.org/10.1002/eqe.369.

Ansari, M., Ansari, M. and Safiey, A. (2018), "Evaluation of seismic performance of mid-rise reinforced concrete frames subjected to far-field and near-field ground motions", *Earthq. Struct.*, **15**(5), 453-462. https://doi.org/10.12989/eas.2018.15.5.453.

Ashrafi, H.R., Amiri, A.M., Dadgar, S. and Beiranvand, P. (2016). "Studying the effects of earthquakes near and far fault region on seismic behavior of dual frame equipped with viscous damper", *Proceedings of the Vibroengineering Procedia*, 23-28.

Beiraghi, H., Kheyroddin, A. and Kafi, M.A. (2016), "Forward directivity near-fault and far-fault ground motion effects on the behavior of reinforced concrete wall tall buildings with one and more plastic hinges", *Struct. Des. Tall Spec. Build.*, **25**(11), 519-539. https://doi.org/10.1002/tal.1270.

Beyen, K. and Tanircan, G. (2015), "Strong ground motion characteristics of the 2011 Van Earthquake of Turkey: Implications of seismological aspects on engineering parameters", *Earthq. Struct.*, **8**(6), 1363-1386. http://dx.doi.org/10.12989/eas.2015.8.6.1363.

BHRC (2014). Iranian Code of Practice for Seismic Resistant Design of Buildings, Standard 2800, 4th Edition. (in Persian)

Bray, J.D. and Rodriguez-Marek, A. (2004), "Characterization of forward-directivity ground motions in the near-fault region", *Soil Dyn. Earthq. Eng.*, **24**(11), 815-828. https://doi.org/10.1016/j.soildyn.2004.05.001.

Champion, C. and Liel, A. (2012), "The effect of near-fault directivity on building seismic collapse risk", *Earthq. Eng. Struct. Dyn.*, **41**(10), 1391-1409. https://doi.org/10.1002/eqe.1188.

Decanini, L., Mollaioli, F. and Saragoni, R. (2000), "Energy and displacement demands imposed by near-source ground motions", *Proceedings of the 12th World Conference on Earthquake Engineering*.

Dimakopoulou, V., Fragiadakis, M. and Spyrakos, C. (2013), "Influence of modeling parameters on the response of degrading systems to near-field ground motions", *Eng. Struct.*, **53**, 10-24. https://doi.org/10.1016/j.engstruct.2013.03.008.

Esfahanian, A. and Aghakouchak, A.A. (2015), "On the improvement of inelastic displacement demands for near-fault ground motions considering various faulting mechanisms", *Earthq. Struct.*, **9**(3), 673-698. https://doi.org/10.12989/eas.2015.9.3.673.

Eskandari, R., Vafaei, D., Vafaei, J. and Shemshadian, M.E. (2017), "Nonlinear static and dynamic behavior of reinforced concrete steel-braced frames", *Earthq. Struct.*, **12**(2), 191-200. https://doi.org/10.12989/eas.2017.12.2.191.

Etemadi Mashhadi, M.R. (2015), "Development of fragility curves for seismic assessment of steel structures with consideration of soil-structure interaction", M.Sc. Thesis, University of Birjand, Iran.

Farzampour, A. (2019), "Evaluating shear links for use in seismic structural fuses", Doctoral Dissertation, Virginia Tech, United States.

Farzampour, A. and Kamali-Asl, A. (2015), "Seismic hazard assessment for two cities in Eastern Iran", *Earthq. Struct.*, **8**(3), 681-697. https://doi.org/10.12989/eas.2015.8.3.681.

Farzampour, A. and Kamali Asl, A. (2014). "On seismic hazard analysis of the two vulnerable regions in Iran: deterministic and probabilistic approaches", *Proceedings of the 2014 NZSEE Conference, New Zealand*, New Zealand.

Gerami, M. and Abdollahzadeh, D. (2015), "Vulnerability of steel moment-resisting frames under effects of forward directivity", *Struct. Des. Tall Spec. Build.*, **24**(2), 97-122. https://doi.org/10.1002/tal.1156.

Gillie, J.L., Rodriguez-Marek, A. and McDaniel, C. (2010), "Strength reduction factors for near-fault forward-directivity ground motions", *Eng. Struct.*, **32**(1), 273-285. https://doi.org/10.1016/j.engstruct.2009.09.014.

Gupta, A. and Krawinkler, H. (1999), "Seismic demands for performance evaluation of steel moment resisting frame structures", Report No. 132, The John A. Blume Earthquake Engineering Research Center, Stanford University, USA.

Kalkan, E. and Kunnath, S.K. (2006), "Effects of fling step and forward directivity on seismic response of buildings", *Earthq. Spectra*, **22**(2), 367-390. https://doi.org/10.1193/1.2192560.

Khorami, M., Khorami, M., Alvansazyazdi, M., Shariati, M., Zandi, Y., Jalali, A. and Tahir, M.M. (2017), "Seismic performance evaluation of buckling restrained braced frames (BRBF) using incremental nonlinear dynamic analysis method (IDA)", *Earthq. Struct.*, **13**(6), 531-538.

Khoshnoudian, F. and Ahmadi, E. (2013), "Effects of pulse period of near-field ground motions on the seismic demands of soil-MDOF structure systems using mathematical pulse models", *Earthq. Eng. Struct. Dyn.*, **42**(11), 1565-1582. https://doi.org/10.1002/eqe.2287.

Landolfo, R., Mazzolani, F., Dubina, D., da Silva, L.S. and D'Aniello, M. (2017), *Design of Steel Structures for Buildings*

in Seismic Areas, 1st Edition, Ernst & Sohn, Portugal.

Lignos, D.G. and Krawinkler, H. (2009), "Sidesway collapse of deteriorating structural systems under seismic excitations", Report No. TB 172, The John A. Blume Earthquake Engineering Research Center, Stanford University, USA.

Mansouri, I., Safa, M., Ibrahim, Z., Kisi, O., Tahir, M.M., Baharom, S. and Azimi, M. (2016), "Strength prediction of rotary brace damper using MLR and MARS", *Struct. Eng. Mech.*, **60**(3), 471-488. https://doi.org/10.12989/sem.2016.60.3.471.

Mirzai, N.M., Attarnejad, R. and Hu, J.W. (2018), "Enhancing the seismic performance of EBFs with vertical shear link using a new self-centering damper", *Ing. Sismica*, **35**(4), 57-76.

Moniri, H. (2017), "Evaluation of seismic performance of reinforced concrete (RC) buildings under near-field earthquakes", *Int. J. Adv. Struct. Eng.*, **9**(1), 13-25. https://doi.org/10.1007/s40091-016-0145-6.

Mortezaei, A. and Ronagh, H.R. (2013), "Plastic hinge length of reinforced concrete columns subjected to both far-fault and near-fault ground motions having forward directivity", *Struct. Des. Tall Spec. Build.*, **22**(12), 903-926. https://doi.org/10.1002/tal.729.

Nastri, E., Montuori, R. and Piluso, V. (2015), "Seismic design of MRF-EBF dual systems with vertical links: EC8 vs plastic design", *J. Earthq. Eng.*, **19**(3), 480-504. https://doi.org/10.1080/13632469.2014.978917.

Nastri, E., Vergato, M. and Latour, M. (2017), "Performance evaluation of a seismic retrofitted R.C. precast industrial building", *Earthq. Struct.*, **12**(1), 13-21.

Nicknam, A., Barkhodari, M.A., Jamnani, H.H. and Hosseini, A. (2013), "Compatible seismogram simulation at near source site using Multi-Taper Spectral Analysis approach (MTSA)", *J. Vib.*, **15**(2), 626-638. https://doi.org/10.12989/eas.2017.12.1.013.

Ohtori, Y., Christenson, R.E., Spencer Jr, B.F. and Dyke, S.J. (2004), "Benchmark control problems for seismically excited nonlinear buildings", *J. Eng. Mech.*, **130**(4), 366-385. https://doi.org/10.1061/(ASCE)0733-9399(2004)130:4(366).

PEER/ATC-72-1 (2010), Modeling and Acceptance Criteria for Seismic Design and Analysis of Tall Buildings, Applied Technology Council, Redwood City, California.

Rahgozar, N., Moghadam, A.S. and Aziminejad, A. (2017), "Response of self-centering braced frame to near-field pulse-like ground motions", *Struct. Eng. Mech.*, **62**(4), 497-506. https://doi.org/10.12989/sem.2017.62.4.497.

Seo, J., Dueñas-Osorio, L., Craig, J.I. and Goodno, B.J. (2012), "Metamodel-based regional vulnerability estimate of irregular steel moment-frame structures subjected to earthquake events", *Eng. Struct.*, **45**, 585-597. https://doi.org/10.1016/j.engstruct.2012.07.003.

Seo, J. and Hu, J.W. (2016), "Seismic response and performance evaluation of self-centering LRB isolators installed on the CBF building under NF ground motions", *Sustain. (Switzerland)*, **8**(2), 1-22. https://doi.org/10.3390/su8020109.

Seo, J., Hu, J.W. and Davaajamts, B. (2015a), "Seismic performance evaluation of multistory reinforced concrete moment resisting frame structure with shear walls", *Sustain. (Switzerland)*, **7**(10), 14287-14308. https://doi.org/10.3390/su71014287.

Seo, J., Kim, Y.C. and Hu, J.W. (2015b), "Pilot study for investigating the cyclic behavior of slit damper systems with recentering shape memory alloy (SMA) bending bars used for seismic restrainers", *Appl. Sci. (Switzerland)*, **5**(3), 187-208. https://doi.org/10.3390/app5030187.

Seo, J. and Shukla, R. (2016). "Joint seismic and scour fragility assessment of a steel building incorporating soil-structure interaction", *Proceedings of the Geotechnical and Structural Engineering Congress 2016-Proceedings of the Joint Geotechnical and Structural Engineering Congress 2016*, 1941-1951.

Shahbazi, S., Khatibinia, M., Mansouri, I. and Hu, J.W. (2018a), "Seismic evaluation of special steel moment frames undergoing near-field earthquakes with forward directivity by considering soil-structure interaction effects", *Sci. Iranica*. https://doi.org/10.24200/SCI.2018.50241.1594 . (in Press)

Shahbazi, S., Mansouri, I., Hu, J.W. and Karami, A. (2018b), "Effect of soil classification on seismic behavior of SMFs considering soil-structure interaction and near-field earthquakes", *Shock Vib.*, **2018**, Article ID 4193469, 17. https://doi.org/10.1155/2018/4193469.

Shahbazi, S., Mansouri, I., Hu, J.W., Sam Daliri, N. and Karami, A. (2019), "Seismic response of steel SMFs subjected to vertical components of far- and near-field earthquakes with forward directivity effects", *Adv. Civ. Eng.*, **2019**, Article ID 2647387, 15. https://doi.org/10.1155/2019/2647387.

Singh, J.P. (1985), "Earthquake ground motions: Implications for designing structures and reconciling structural damage", *Earthq. Spectra*, **1**(2), 239-270. https://doi.org/10.1193/1.1585264.

Tajammolian, H., Khoshnoudian, F. and Bokaeian, V. (2016), "Seismic responses of asymmetric steel structures isolated with the TCFP subjected to mathematical near-fault pulse models", *Smart Struct. Syst.*, **18**(5), 931-953. http://dx.doi.org/10.12989/sss.2016.18.5.931.

Tajammolian, H., Khoshnoudian, F., Talaei, S. and Loghman, V. (2014), "The effects of peak ground velocity of near-field ground motions on the seismic responses of base-isolated structures mounted on friction bearings", *Earthq. Struct.*, **7**(6), 1259-1281. http://dx.doi.org/10.12989/eas.2014.7.6.1259.

Veismoradi, S. and Darvishan, E. (2018), "Probabilistic seismic assessment of mega buckling-restrained braced frames under near-fault ground motions", *Earthq. Struct.*, **15**(5), 487-498. https://doi.org/10.12989/eas.2018.15.5.487.

Yazdani, Y. and Alembagheri, M. (2017), "Nonlinear seismic response of a gravity dam under near-fault ground motions and equivalent pulses", *Soil Dyn. Earthq. Eng.*, **92**, 621-632. https://doi.org/10.1016/j.soildyn.2016.11.003.

Yin, S., Li, Y., Sandberg, M. and Lam, K. (2017), "The effect of building spacing on near-field temporal evolution of triple building plumes", *Build. Environ.*, **122**, 35-49. https://doi.org/10.1016/j.buildenv.2017.05.030.

Zeynali, K., Saeed Monir, H., Mirzai, N.M. and Hu, J.W. (2018), "Experimental and numerical investigation of lead-rubber dampers in chevron concentrically braced frames", *Arch. Civil Mech. Eng.*, **18**(1), 162-178. https://doi.org/10.1016/j.acme.2017.06.004.

Zhao, D., Liu, Y. and Li, H. (2017), "Self-tuning fuzzy control for seismic protection of smart base-isolated buildings subjected to pulse-type near-fault earthquakes", *Appl. Sci. (Switzerland)*, **7**(2), 185. https://doi.org/10.3390/app7020185.

CC